ISSN (Print) 1226-1750
ISSN (Online) 2233-6656
**Journal of Magnetics** 27(1), 106-115 (2022) https://doi.org/10.4283/JMAG.2022.27.1.106

# Magnetic Characteristics of Biological Fluid in Nonlinear Thermally Radiated Blood Flow

**Bilal Ahmed[1], Sami Ullah Khan[2], M. Ijaz Khan[3,4]*, Soumaya Gouadria[5], Abdul H. Hamid[6], Mehreen Yousaf[7], and M. Y. Malik[8]**

*[1]Department of Mathematics and Statistics, The University of Lahore, Sargodha Campus 40100, Pakistan*
*[2]Department of Mathematics, COMSATS University Islamabad, Sahiwal 57000, Pakistan*
*[3]Department of Mathematics and Statistics, Riphah International University I-14, Islamabad 44000, Pakistan*
*[4]Mathematical Modelling and Applied Computation Research Group (MMAC), Department of Mathematics, King Abdulaziz University, Jeddah, Saudi Arabia*
*[5]Department of Physics, College of Science, Princess Nourah bint Abdulrahman University, P.O. Box 84428, Riyadh 11671, Saudi Arabia*
*[6]Department of Mathematics, Division of Science and Technology, University of Education, Lahore, Pakistan*
*[7]DHQ Hospital Sahiwal, Punjab Pakistan*
*[8]Department of Mathematics, College of Sciences, King Khalid University, Abha 61413, Saudi Arabia*

(Received 11 October 2021, Received in final form 9 February 2022, Accepted 10 February 2022)

**The numerical solution of the flow non-Newtonian fluid induced by stretching sheet in the region of oblique stagnation point flow under inducement of externally applied uniform magnetic field orthogonal to the flow is presented. The analysis is made under the assumption of boundary layer which arrives to the system of partial differential equations which are then transformed to ordinary differential equations by using appropriate similarity transformations. The numerical solution of the modeled system of equation is obtained by parallel shooting technique and presented for different variations of involved parameters. It is noted that enhancement in magnetic field results in decrease in horizontal velocity and boundary layer becomes thinner. The obtained results are compared with the available results in the literature and found in excellent agreement in the limiting cases.**

**Keywords :** thermal radiation, uniform magnetic field, maxwell fluid, oblique stagnation point

## 1. Introduction

The stagnation point flow when fluid moves the local velocity the fluid will be zero. In the flow fluid stagnation point exist the surface of body, the fluid of the body well be rest. The oblique stagnation point flow discussed and combined at a plane wall are positions to free restriction. Stagnation point flow at oblique flow consist an orthogonal flow which added a shear flow the infinite velocity is immovable. A stagnation point is considered when fluid collides with the surface and the velocity of fluid vanishes i.e. becomes zero. Recently many researchers taking more interest in stagnation point flows due to numerous applied applications in industry. Cooling of nuclear reactor is example of stagnation flow. In stagnation flow, the attentionable thing is that the greatest heat moves and pressure gradient is found at stagnation stage. Initially Stuart (1959) worked on stagnation flow obtained the analytical solutions for the flow. Tamada [1] and Dorrepaal [2] presented the generalized flow involving stagnation point and obtained solution for oblique stagnation point. Husain *et al*. [3] worked on continuous the work viscoelastic fluid model in stagnation point flow.

The non-Newtonian fluid model is more difficult and complex to solve the single constitutive equation but Newtonian fluid model is easily to solve the single constitutive equation. Moreover, purpose of many researches descries their application, Maxwell sees the proposal they attention of simplicity of viscoelastic fluid. Wang and Tan [4] studied the linear stability explanation by Maxwell fluid model with thermal diffusion effect. The oscillatory convection damaged system by thermal diffusion and


*Corresponding author: Tel: +92-300-9019713
e-mail: mikhan@math.qau.edu.pk

undependability of rise system due to increase time composure. Javed *et al*. [5] in Maxwell fluid, the more suggested flow of stagnation point is comprehensive. Mukhopadhyay [6] visualized the heat source importance for Maxwell fluid. Nadeem *et al*. [7] provided are generalized literature. The most important stretching surface used by industrial firms, such as warm progression, metal sheet freezing, crystal fibers, wire drawing, and various other materials.

A flow model solves boundary layer approximation by non-linear equation like continuous and momentum transformation. Khan *et al*. [8] generalized diffusion effects on Maxwell nanofluid stagnancy point flow over an extended sheet with chemical reaction in slip conditions. Jawad *et al*. [9] studied the partition of Non-linear thermal radiation and sticky carelessly effect on the time independent which rotating in three-dimensional flow of single wall carbon nanotubes with sedimentary suspensions. Majeed *et al*. [10] studied the influence of rotate the magnetic field on Maxwell concentrated ferrofluid flow over a heated widening sheet with heat generation. Reza-E-Rabbi *et al*. [11] the fluid flow behavior over a stretching sheet computational modeling of multiphase radiative Casson and Maxwell fluid the appearance of nano-size particles. Li *et al*. [12] the nanofluid in oblique stagnation point flow of stretching/shrinking sheet with Cattaneo-Christov heat flux model to develop the equation of energy and investigate the equation of surface heat transfer. Ali *et al*. [13] estimated the flow of time independent Eyring-Powell nanofluid closed to stagnancy point elapsed a convectively heated widening sheet. Patel [14]. The heat generation and cross diffusion on combined convective magneto-hydrodynamics flow of Casson fluid through impermeable medium thermal radiation with non-linear. Sobamowo *et al*. [15] the study on the impacts of the inclined magnetic flied flow medium porosity then thermal energy in the heat moves and free convection flow of Casson nanofluid a vertical plate. Ghaffari *et al*. [16] in this study simulation and decoration natural convection flow along a vertical wavy of surface of sinusoidal natural with heat flux. Vijaya *et al*. [17] performed investigation the problem of oblique hydro magnetic stagnation flow of point an electrically Casson fluid over a stretching sheet embedded in a doubly stratified medium in the present of heat source and thermal radiation with first chemical reaction. Javed *et al*. [18] discussed numerical analysis mixed convection boundary layer flow second grand viscoelastic due to cylinder of elliptic cross section with prescribed surface heat flux. Ibrahim *et al*. [19] presented study slip effect stagnation point flow of upper converted non-Newtonian fluid of nanofluid passing a stretching sheet with chemical reaction. Hayat *et al.* [20] used the boundary condition of Maxwell fluid in study flow of fluid with convective. Mushtaq *et al.* [21] determined the numerical solution of Sakiadis flow fluid for upper surface plate of non-Newtonian fluid using Cattaneo-Christove model of heat flux. Awad *et al.* [22] continued the investigation of linear stability of non-Newtonian fluid with the cross-diffusion and double diffusive convection in a horizontal layer.

In present problem study of boundary layer oblique stagnation point flow of Maxwell fluid with radiation effects over a linear stretching sheet under the inducement of magnetic field has been carried out. Themodeling and numerical simulation by using parallel shooting technique of governing equations are presented. Effects of different involved parameter on heat and fluid flow are presented through tables and graphs and detail discussion is given in the later part of the manuscript. An excellent agreement of results has been found with Pop *et al.* [23] and Javed and Ghaffari [5]. Refs. [24-30] summarize some important result regarding fluid flow.

## 2. Mathematical Modeling

Consider two dimensional steady flow of Maxwell fluid over a stretching sheet in the region of non-orthogonal stagnation point under the influence of externally applied uniform magnetic field orthogonal to the flow. The stretching sheet is assumed along the plane $y = 0$ and the flow moves along the $y$-axis. The velocity $U_w = cx$ is the stretching velocity of the sheet, with $c(> 0)$ being the stretch constant.

The governing equations in the presence of body forces that describes the current flow are,

$$div\bar{V} = 0, \tag{1}$$

$$\rho\frac{d\bar{V}}{dt} = -\nabla p + div\bar{S} + \rho b, \tag{2}$$

$$\bar{u}\frac{\partial\bar{T}}{\partial\bar{x}} + \bar{v}\frac{\partial\bar{T}}{\partial\bar{y}} = \frac{k}{\rho c_p}\bar{\nabla}^2\bar{T} - \frac{1}{\rho c_p}\bar{\nabla}.q_r. \tag{3}$$

The *div* characterizes the divergence operator, $V=[\bar{u}, \bar{v}, 0]$ is the vector velocity, $\bar{u}$ and $\bar{v}$ are the velocity movement components in the direction of $\bar{x}$ and $\bar{y}$ axis respectively. The bar shows that these quantities are in dimensionless form that will be converted into dimensional form where $\rho$ is the density, $p$ is the pressure, $\kappa$ is the thermal conductivity fluid, $c_p$ is the steady pressure of real heat, $b$ is the is the body force caused by the magnetic field and $q_r$ represents the radiative heat flux and $\bar{S}$ is the extra stress tensor for Maxwell fluid is explain below,

$$q_r = -\frac{4\sigma^*}{3(\alpha_r+\sigma_s)}\frac{\partial \bar{T}^4}{\partial \bar{y}}, \tag{4}$$

$$\bar{S} + \lambda_1 \frac{D\bar{S}}{Dt} = \mu \bar{A}_1, \tag{5}$$

where Stefan Boltzmann's-constant is σ* where $\alpha_r$, $\sigma_s$, $\mu$, and $\bar{\lambda}_1$, the Rosseland definition is the corresponding fluid for dynamic viscosity, scattering coefficient, absorption coefficient, and time relaxation content. $\bar{A}_1$ is the representation of the first tensor by Rivlin Ericksen, explained by,

$$\bar{A}_1 = \bar{L} + \bar{L}^T. \tag{6}$$

The of velocity gradient is $\bar{L}$ and its transpose is defined as,

$$\bar{L} = \begin{pmatrix} \frac{\partial \bar{u}}{\partial \bar{x}} & \frac{\partial \bar{u}}{\partial \bar{y}} & 0 \\ \frac{\partial \bar{v}}{\partial \bar{x}} & \frac{\partial \bar{v}}{\partial \bar{y}} & 0 \\ 0 & 0 & 0 \end{pmatrix} \text{ and } \bar{L}^T = \begin{pmatrix} \frac{\partial \bar{u}}{\partial \bar{x}} & \frac{\partial \bar{v}}{\partial \bar{x}} & 0 \\ \frac{\partial \bar{u}}{\partial \bar{y}} & \frac{\partial \bar{v}}{\partial \bar{y}} & 0 \\ 0 & 0 & 0 \end{pmatrix}. \tag{7}$$

The $D/Dt$ is an operator explained correspondingly in the form of a cotravariant vector and contravariant tensor of rank 2 in Eq. (8) and (9) respectively

$$\frac{DS}{Dt} = \frac{dS}{dt} - \bar{L}\bar{S}, \tag{8}$$

$$\frac{D\bar{S}}{Dt} = \frac{d\bar{S}}{dt} - \bar{L}\bar{S} - \bar{S}\bar{L}^T. \tag{9}$$

Divergence Applied on Eq. (5) yields,

$$\left(1 + \lambda_1 \frac{D}{Dt}\right) \nabla . S = \mu \nabla . \bar{A}_1. \tag{10}$$

Application of $\left(1 + \lambda_1 \frac{D}{Dt}\right)$ on the both side of Eq. (2) yields

$$\left(\rho \frac{d\bar{V}}{dt} + \bar{\nabla} p\right)\left(1 + \lambda_1 \frac{D}{Dt}\right) = \left(1 + \lambda_1 \frac{D}{Dt}\right) div\bar{S} + \left(1 + \lambda_1 \frac{D}{Dt}\right)\rho b, \tag{11}$$

$$\therefore div\bar{S} = \nabla . S \tag{12}$$

so,

$$\left(\rho \frac{d\bar{V}}{dt} + \bar{\nabla} p\right)\left(1 + \lambda_1 \frac{D}{Dt}\right) = \left(1 + \lambda_1 \frac{D}{Dt}\right) \nabla . S + \left(1 + \lambda_1 \frac{D}{Dt}\right)\rho b. \tag{13}$$

The body fore defined in the above equation represents the Lorentz force which can be expressed as

$$b^i = \sigma\left[\overline{V} \times \overline{B}\right] \times \overline{B}. \tag{14}$$

As flow is the $x$-direction and $B_0$ is the strength of uniform constant magnetic field that applied in $y$-direction, therefore we have

$$\overline{B} = \left(0, B_{0,} 0\right). \tag{15}$$

Thus

$$\left(\overline{V} \times \overline{B}\right) \times \overline{B} = (-uB_0^2, 0, 0).$$

and $\overline{V} \times \overline{B} = (0, 0, uB_0)$. (16)

Using Eq. (16) in Eq. (14) yields

$$b^i = (-\sigma u B_0^2, 0, 0) \tag{17}$$

Using Eq. (17) in Eq. (13) and then expressed in component form,

$x$-component,

$$\left(\bar{u}\frac{\partial \bar{u}}{\partial \bar{x}} + \bar{v}\frac{\partial \bar{u}}{\partial \bar{y}}\right) = -\frac{1}{\rho}\frac{\partial p}{\partial \bar{x}} - \frac{\lambda_1}{\rho}\left(\bar{u}\frac{\partial^2 p}{\partial \bar{x}^2} + \bar{v}\frac{\partial^2 p}{\partial \bar{x}\partial \bar{y}} - \frac{\partial \bar{u}}{\partial \bar{x}}\frac{\partial p}{\partial \bar{x}} - \frac{\partial \bar{u}}{\partial \bar{y}}\frac{\partial p}{\partial \bar{y}}\right) + v\left(\frac{\partial^2 \bar{u}}{\partial \bar{x}^2} + \frac{\partial^2 \bar{u}}{\partial \bar{y}^2}\right) - \lambda_1\left(\bar{u}^2\frac{\partial^2 \bar{u}}{\partial \bar{x}^2} + 2\bar{u}\bar{v}\frac{\partial^2 \bar{u}}{\partial \bar{x}\partial \bar{y}} + \bar{v}^2\frac{\partial^2 \bar{u}}{\partial \bar{y}^2}\right) - \sigma u {B_0}^2 + \lambda_1\left(-\sigma {B^2}_0 v\frac{\partial u}{\partial y}\right), \tag{18}$$

$y$-component,

$$\left(\bar{u}\frac{\partial \bar{v}}{\partial \bar{x}} + \bar{v}\frac{\partial \bar{v}}{\partial \bar{y}}\right) = -\frac{1}{\rho}\frac{\partial p}{\partial \bar{y}} - \frac{\lambda_1}{\rho}\left(\bar{v}\frac{\partial^2 p}{\partial \bar{y}^2} + \bar{u}\frac{\partial^2 p}{\partial \bar{x}\partial \bar{y}} - \frac{\partial \bar{v}}{\partial \bar{x}}\frac{\partial p}{\partial \bar{x}} - \frac{\partial \bar{v}}{\partial \bar{y}}\frac{\partial p}{\partial \bar{y}}\right) + v\left(\frac{\partial^2 \bar{v}}{\partial \bar{x}^2} + \frac{\partial^2 \bar{v}}{\partial \bar{y}^2}\right) - \lambda_1\left(\bar{u}^2\frac{\partial^2 \bar{v}}{\partial \bar{x}^2} + \overline{2u}\bar{v}\frac{\partial^2 \bar{v}}{\partial \bar{x}\partial \bar{y}} + \bar{v}^2\frac{\partial^2 \bar{v}}{\partial \bar{y}^2}\right) + \lambda_1\left(\sigma {B^2}_0 u\frac{\partial v}{\partial x}\right). \tag{19}$$

The boundary conditions are given below in the present flow problem.

$$\left.\begin{array}{lll} \bar{u} = \bar{c}\bar{x}, & \bar{v} = 0 & \text{at } \bar{y} = 0 \\ \bar{u} = a\bar{x} + b\bar{y}, & & \text{as } \bar{y} \to \infty, \end{array}\right\} \tag{20}$$

The Eqs. (19) and (20) reduced by using boundary layer approximation as follows

$$\left(\bar{u}\frac{\partial \bar{u}}{\partial \bar{x}} + \bar{v}\frac{\partial \bar{u}}{\partial \bar{y}}\right) = -\frac{1}{\rho}\frac{\partial p}{\partial \bar{x}} - \frac{\lambda_1}{\rho}\left(\bar{u}\frac{\partial^2 p}{\partial \bar{x}^2} + \bar{v}\frac{\partial^2 p}{\partial \bar{x}\partial \bar{y}} - \frac{\partial \bar{u}}{\partial \bar{x}}\frac{\partial p}{\partial \bar{x}} - \frac{\partial \bar{u}}{\partial \bar{y}}\frac{\partial p}{\partial \bar{y}}\right) + v\left(\frac{\partial^2 \bar{u}}{\partial \bar{x}^2} + \frac{\partial^2 \bar{u}}{\partial \bar{y}^2}\right) - \lambda_1\left(\bar{u}^2\frac{\partial^2 \bar{u}}{\partial \bar{x}^2} + 2\bar{u}\bar{v}\frac{\partial^2 \bar{u}}{\partial \bar{x}\partial \bar{y}} + \bar{v}^2\frac{\partial^2 \bar{u}}{\partial \bar{y}^2}\right) + \frac{\sigma {B^2}_0}{\rho}\left(-u - \lambda_1 v\frac{\partial u}{\partial y}\right). \tag{21}$$

In order to get the simulation of the modeled governing equations one need to transform the governing equations by using appropriate similarity transformation given as,

$$\left.\begin{array}{c} \bar{x} = x\sqrt{\frac{v}{c}},\ \bar{y} = y\sqrt{\frac{v}{c}},\ \bar{u} = u\sqrt{cv},\ \bar{v} = v\sqrt{cv}, \\ \bar{T} = T, \quad T_w = \Delta T + T_\infty \quad p = \rho c v P \end{array}\right\} \tag{22}$$

Eq. (21) in dimensionless from becomes

$$\left(u\frac{\partial u}{\partial x}+v\frac{\partial u}{\partial y}\right)=-\frac{\partial P}{\partial x}+\beta\left(\frac{\partial u}{\partial y}\frac{\partial P}{\partial y}\right)+\left(\frac{\partial^2 u}{\partial y^2}\right)-\beta\left(u^2\frac{\partial^2 u}{\partial x^2}+2uv\frac{\partial^2 u}{\partial x\partial y}+v^2\frac{\partial^2 u}{\partial y^2}\right)+M^2\left(-u-\lambda_1 cv\frac{\partial u}{\partial y}\right). \quad (23)$$

Boundary conditions take the form as given

$$u=x,\quad v=0\quad \text{at}\quad y=0 \quad (24)$$

$$u=\frac{a}{c}x+\frac{b}{c}y,\qquad \text{as}\quad y\to\infty \quad (25)$$

Now, for heat transfer analysis, assume that $T_\infty$ is the temperature of the fluid while the temperature of the stretching surface is represented by $T_w$. By using the transformation given in Eq. (22) and Eq. (4), Eq. (3) becomes

$$\left(u\frac{\partial T}{\partial x}+v\frac{\partial T}{\partial y}\right)=\frac{1}{Pr}\frac{\partial}{\partial y}\left(\left(1+\frac{4}{3}Rd\left((\theta_w-1)T+1\right)^3\right)\frac{\partial T}{\partial y}\right). \quad (26)$$

The boundary conditions dare,

$$\left.\begin{array}{l} T=1\quad \text{at}\quad y=0 \\ T=0\quad \text{as}\quad y\to\infty \end{array}\right\} \quad (27)$$

Where $\beta=\lambda_1 c$ is Deborah number which represents the fluidity of the material, $Pr=\mu c_p/k$ is the Prandtl number, $M^2=\sigma B_0{}^2/\rho$ be the Hartmann number, $Rd=4\sigma^* T_\infty^3/k(\alpha_r+\sigma_s)$ and $q_w=T_w/T_\infty$ represents the temperature of the surface. The stream functionψthat will be used in the governing equations, as shown below,

$$u=\frac{\partial \psi}{\partial y}\ ,\quad v=-\frac{\partial \psi}{\partial x}, \quad (28)$$

Using Eq. (23) to (27) and (26),

$$\frac{\partial\psi}{\partial y}\frac{\partial^2\psi}{\partial x\partial y}-\frac{\partial\psi}{\partial x}\frac{\partial^2\psi}{\partial y^2}+\beta\left(\left(\frac{\partial\psi}{\partial y}\right)^2\frac{\partial^3\psi}{\partial y^3}-2\frac{\partial\psi}{\partial y}\frac{\partial\psi}{\partial x}\frac{\partial^3\psi}{\partial x\partial y^2}+\left(\frac{\partial\psi}{\partial x}\right)^2\frac{\partial^3\psi}{\partial x^2\partial y}\right)=-\frac{\partial P}{\partial x}+\beta\left(\frac{\partial^2\psi}{\partial y^2}\frac{\partial P}{\partial y}\right)+\left(\frac{\partial^3\psi}{\partial y^3}\right)+M^2\left(-\frac{\partial\psi}{\partial y}+\beta\frac{\partial\psi}{\partial x}\frac{\partial^2\psi}{\partial y^2}\right), \quad (29)$$

$$\left(\frac{\partial\psi}{\partial y}\frac{\partial T}{\partial x}-\frac{\partial\psi}{\partial x}\frac{\partial T}{\partial y}\right)=\frac{1}{Pr}\frac{\partial}{\partial y}\left(\left(1+\frac{4}{3}Rd\left((\theta_w-1)T+1\right)^3\right)\frac{\partial T}{\partial y}\right), \quad (30)$$

$$\psi=0,\quad \frac{\partial\psi}{\partial y}=x,\quad T=1\quad \text{at}\quad y=0 \quad (31)$$

$$\psi=\frac{a}{c}xy+\frac{1}{2}\gamma y,\quad T=0\quad \text{as}\quad y\to\infty \quad (32)$$

where $\gamma=b/c$ denotes shear in the free stream of the flow. Suppose the solution of Eqs. (29) and (30) subject to boundary conditions Eq. (31) and (32) is of the form,

$$\psi=x\tilde{f}(y)+\tilde{g}(y),\quad T=\tilde{\theta}(y). \quad (33)$$

The functions $\tilde{f}(y)$ and $\tilde{g}(y)$ are the oblique and normal elements of the streams. Using Eq. (33) in Eqs. (29) to (32) we have,

$$\left(x\tilde{f}'(y)+\tilde{g}'(y)\right)\tilde{f}'(y)-\tilde{f}(y)\left(x\tilde{f}''(y)+\tilde{g}''(y)\right)+\beta\left(\left(\tilde{f}(y)\right)^2\left(x\tilde{f}'''(y)+\tilde{g}'''(y)\right)-2\tilde{f}(y)\left(x\tilde{f}'(y)+\tilde{g}'(y)\tilde{f}''(y)\right)\right)=-\frac{\partial P}{\partial x}+\beta\left(x\tilde{f}''(y)+\tilde{g}''(y)\right)\frac{\partial P}{\partial y}+x\tilde{f}'''(y)+\tilde{g}'''(y)+M^2\left(-\left(x\tilde{f}'(y)+\tilde{g}'(y)\right)+\beta\tilde{f}(y)\left(x\tilde{f}''(y)+\tilde{g}''(y)\right)\right), \quad (34)$$

$$\frac{\partial}{\partial y}\left(\left(1+\frac{4}{3}Rd\left((\theta_w-1)\tilde{\theta}+1\right)^3\right)\tilde{\theta}'\right)+Pr\tilde{f}(y)\tilde{\theta}'=0, \quad (35)$$

$$\tilde{f}(y)=0,\quad \tilde{f}'(y)=1,\quad \tilde{g}(y)=0,\quad \tilde{g}'(y)=0,\quad \tilde{\theta}(y)=1\quad \text{at}\quad y=0 \quad (36)$$

$$\tilde{f}'(y)=\frac{a}{c},\ \tilde{g}'(y)=\gamma y,\ \tilde{\theta}(y)=0,\ \text{as}\ y\to\infty \quad (37)$$

Aftereliminating the pressurefrom Eq. (34), it takes the form as follows,

$$\left(x\tilde{f}'(y)+\tilde{g}'(y)\right)\tilde{f}'(y)-\tilde{f}(y)\left(x\tilde{f}''(y)+\tilde{g}''(y)\right)+\beta\left(\left(\tilde{f}(y)\right)^2\left(x\tilde{f}'''(y)+\tilde{g}'''(y)\right)-2\tilde{f}(y)\left(x\tilde{f}'(y)+\tilde{g}'(y)\tilde{f}''(y)\right)\right)=-A\gamma+x\left(\frac{a}{c}\right)^2+x\tilde{f}'''(y)+\tilde{g}'''(y)+M^2\left(\frac{a}{c}\right)x+M^2\left(-\left(x\tilde{f}'(y)+\tilde{g}'(y)\right)+\beta\tilde{f}(y)\left(x\tilde{f}''(y)+\tilde{g}''(y)\right)\right), \quad (38)$$

where $M^2=\sigma B_0^2/\rho$. Now by comparing the coefficient as $x^1$ and $x^0$ in Eq. (38), one can have

$$\tilde{f}'''+\left(\frac{a}{c}\right)^2-\tilde{f}'^2+\tilde{f}\tilde{f}''-\beta\left(\tilde{f}^2\tilde{f}'''-2\tilde{f}\tilde{f}'\tilde{f}''-M^2\tilde{f}\tilde{f}''\right)+\left(\frac{a}{c}\right)M^2-M^2\tilde{f}'=0, \quad (39)$$

$$\tilde{g}'''+\tilde{g}''\tilde{f}-\tilde{g}'\tilde{f}'-\beta\left(\tilde{f}^2\tilde{g}''-2\tilde{f}\tilde{g}'\tilde{f}''-M^2\tilde{g}''\tilde{f}\right)-M^2\tilde{g}'=A\gamma, \quad (40)$$

where boundary layer displacement is represented by $A$. Now for more simplification using a new variable is introduced which is defined as

$$\tilde{g}'(y) = \gamma\tilde{h}(y) \tag{41}$$

Eq. (38) and the associated boundary condition are reduce to

$$\tilde{h}'' + \tilde{h}'\tilde{f} - \tilde{h}\tilde{f}' - \beta\left(\tilde{f}^2\tilde{h}'' - 2\tilde{f}\tilde{h}\tilde{f}'' - M^2\tilde{h}'\tilde{f}\right) - M^2\tilde{h} = A \tag{42}$$

$$\tilde{h}(y) = 0 \quad \text{at} \quad y = 0, \tag{43}$$

$$\tilde{h}'(y) = 1 \quad \text{as} \quad y \to \infty \tag{44}$$

The local Nusselt number of physical quantities is defined below as,

$$Nu_x = \frac{\bar{x}q_w}{k(T_w - T_\infty)}, \tag{45}$$

where

$$q_w = -\left[\left(\frac{4}{3}\frac{4\sigma^*\bar{T}^3}{(\alpha_r+\sigma_s)} + k\right)\frac{\partial\bar{T}}{\partial\bar{y}}\right]. \tag{46}$$

Using dimensionless variables and transformation given in Eq. (22) the above equation reduces to,

$$Nu_x(Re_x)^{\frac{-1}{2}} = -\left[\left(\frac{4}{3}Rd(\theta_w)^3 + 1\right)\tilde{\theta}'\right]. \tag{47}$$

It is worth mention here that limiting case for Newtonian case can be obtained by placing $\beta = 0$ and case orthogonal stagnation point flow can also be obtained by placing $\gamma = 0$.

## 3. Numerical Method

Using the boundary condition (36), (37), (43) and (44) in the Non-linear equation of (35), (39), and (42). They solve these equations in Numerical with parallel shooting method. The simple shooting method is very easy in the compare of parallel shooting method but simple shooting method is very difficult to solve higher non-linear problems. That way we used parallel shooting. The parallel method of shooting is well-organized for. The technique is described as below,

(i) Equations (35), (39) and (42)are reduced to the first order of differential equations by letting

(ii) $\tilde{f} = f_1$ , $h = f_4$ , $\tilde{h}' = f_5$ , $\tilde{\theta} = f_6$,

$$f_1' = f_2 \text{ , } f_2' = f_3 \text{ ,}$$

$$f_3' = \frac{1}{1-\beta{f_1}^2}\left({f_2}^2 - \left(\frac{a}{c}\right)^2 - f_1 f_3 - \beta(2\beta f_1 f_2 f_3 + M^2 f_1 f_3) - \left(\frac{a}{c}\right)M^2 + M^2 f_2\right), \tag{48}$$

$$f_4' = f_5 \text{ ,}$$

$$f_5' = \frac{1}{1-\beta{f_1}^2}\left(-f_1 f_5 - \beta\left(2f_1 f_3 f_4 + \sigma{B_0}^2 f_1 f_5\right) + \sigma{B_0}^2 f_4 + A\right), \tag{49}$$

$$f_6' = f_7 \text{ ,}$$

$$f_7' = \frac{1}{1+\frac{4}{3}Rd(1+(\theta_w-1)f_6)^3}\left(\begin{matrix}(-4Rd(\theta_w-1)(1+(\theta_w-1)f_6)^2)(f_7)^2 \\ -Prf_1f_7\end{matrix}\right). \tag{50}$$

The boundary conditions are given below,

$$f_1(0) = 0, \quad f_2(0) = 1, \quad f_2(y_\infty) = \frac{a}{c}, \tag{51}$$

$$f_4(0) = 0, \qquad f_5(y_\infty) = 1, \tag{52}$$

(iii) The considered domain from 0 to $y_\infty$ is divided into the '$n$' number of intervals where '$n$' depends strictly on required convergence of the solution.

(iv) The problem is solved for first interval by setting suitable initial guess and obtained solution is considered as initial guess for next interval and this process is carried out until the solution for the last interval is obtained.

(v) The solution for each interval is obtained such that is satisfies the boundary condition at $y_\infty$.

(vi) The algorithm is self-developed in MATLAB R2015a.

## 4. Results and Discussion

The Eqs. (35), (39) and (42) with appropriate conditions given in Eqs. (36), (37), (43) and (44) have been solved by implementing above mentioned scheme for various values of involved parameters $\beta$, $a/c$, $\gamma$ and $M$. To present the accuracy of our present computed results the comparison of $f''(0)$ and $h'(0)$ has been made with Pop *et al.* [23] and Javed and Ghaffari [5] which includes the results for Newtonian and non-Newtonian Maxwell fluid given in Table 1. It is found that our present computed results are highly convergent with Pop *et al.* [23] and Javed and

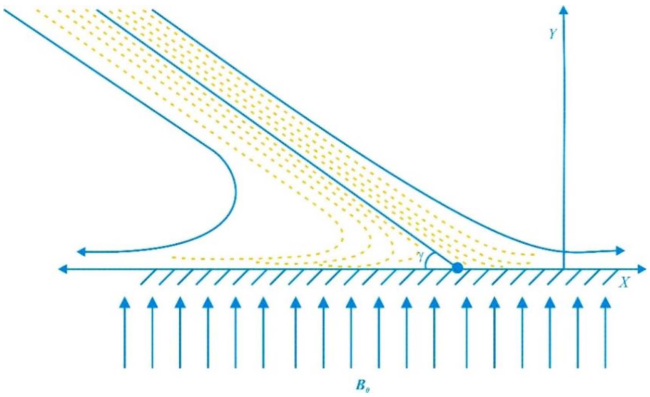


**Fig. 1.** (Color online) Geometry of the considered physical plane.

**Table 1**. The Numerical values of $f''(0)$ and $h'(0)$ for the different values of $\beta$ and $a/c$.

| $a/c$ | Newtonian Fluid ($\beta = 0.0$) | | | Non-Newtonian Fluid ($\beta = 0.2$) | | | | |
|---|---|---|---|---|---|---|---|---|
| | Pop et al. [23] | Javed and Ghaffari [5] | Present | Pop et al. [23] | Ghaffari et al. [5] | Present | Javed and Ghaffari [5] | Present |
| | $f''(0)$ | $f''(0)$ | $f''(0)$ | $f''(0)$ | $f''(0)$ | $f''(0)$ | $h'(0)$ | $h'(0)$ |
| 0.01 | -0.9981 | -0.99802 | -0.9980 | -1.0499 | -1.05009 | -1.0500 | -0.51368 | -0.5137 |
| 0.02 | -0.9958 | -0.99579 | -0.9957 | -10476 | -1.04778 | -1.0477 | -0.24667 | -0.2467 |
| 0.05 | -0.9876 | -0.98758 | -0.9875 | -1.0393 | -1.03939 | -1.0394 | 0.07239 | 0.0724 |
| 0.10 | -0.9694 | -0.96939 | -0.9693 | -1.0207 | -1.02082 | -1.0208 | 0.28154 | 0.2815 |
| 0.20 | -0.9181 | -0.91811 | -0.9181 | -0.96823 | -0.96823 | -0.9683 | 0.49218 | 0.4922 |
| 0.50 | -0.6673 | -0.66726 | -0.6672 | -0.70779 | -0.70779 | -0.7077 | 0.79610 | 0.7961 |
| 1.00 | 0.0000 | 0.0000 | 0.0000 | 0.0000 | 0.0000 | 0.0000 | 1.0000 | 1.0000 |
| 2.00 | 2.0175 | 2.01749 | 2.0175 | 2.2225 | 2.22314 | 2.2231 | 1.09213 | 1.0921 |
| 3.00 | 4.7294 | 4.72824 | 4.7294 | 5.3544 | 5.35217 | 5.3522 | 0.78434 | 0.7843 |
| 5.00 | 11.7537 | 11.75190 | 11.7534 | 14.0144 | 17.00169 | 17.0017 | -2.04649 | -2.0465 |
| 10.0 | 36.2689 | 36.25704 | 36.2699 | 48.3354 | 48.33540 | 48.3354 | -2.34185 | -2.3419 |

Ghaffari [5]. It is clear from the table that the value of $f''(0)$ is increases as we enhance the value of $a/c$ but $h'(0)$ increases at a certain value and then decreased. Figures 2(a) to 2(d) are plotted to present the variation of horizontal velocity $u$ for various values of velocities ration $a/c$ with fixed values of $x$, $\beta$, $M$, $\gamma = 0.0$, 0.5, 1.0 and 5.0. It is seen that the velocity $u$ increase with enhancement of $\gamma$. The Fig. 2(a) represents the orthogonal flow i.e., $\gamma = 0$, wheras Fig. 2(b) to 2(d) shows the non-orthogonal stagnation point flow ($\gamma \neq 0$). It is observed from the figures that there exist two boundary layer structures which depends upon the ratio of straining and

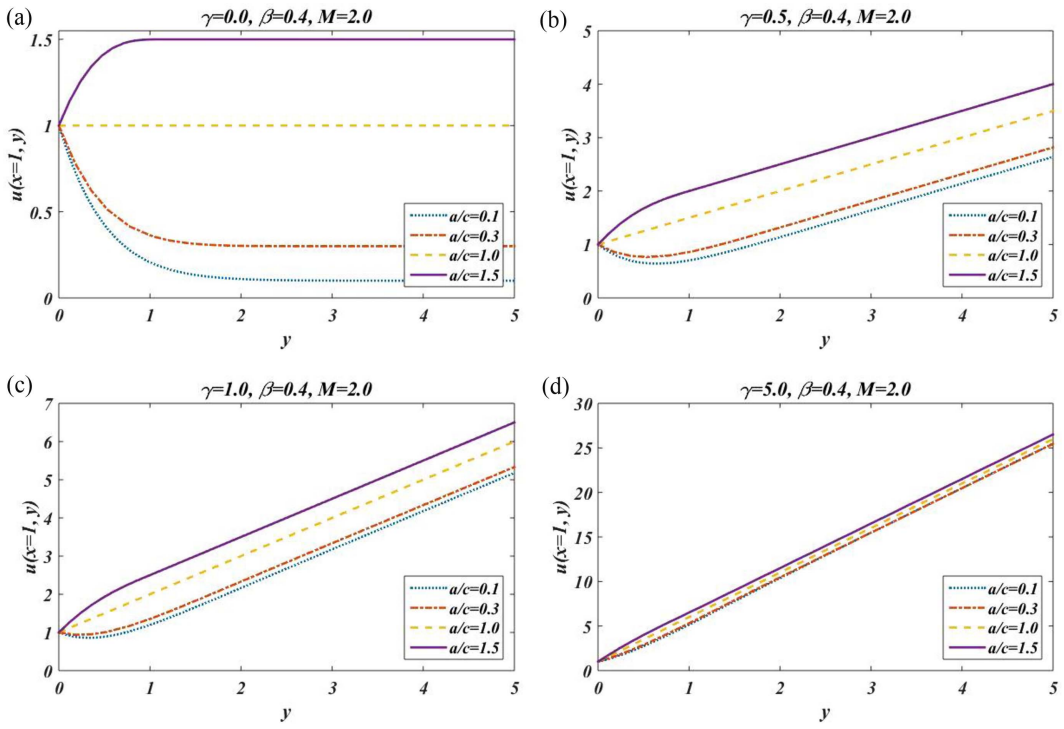


**Fig. 2.** (Color online) (a) Graph of variation of horizontal velocity $u$ along $y$-axis at $x = 1$ for various values of $a/c$ and $\gamma = 0.0$, $\beta = 0.4$ and $M = 2.0$, (b) Graph of variation of horizontal velocity $u$ along $y$-axis at $x = 1$ for various values of $a/c$ and $\gamma = 0.5$, $\beta = 0.4$ and $M = 2.0$, (c) Graph of variation of horizontal velocity $u$ along $y$-axis at $x = 1$ for various values of $a/c$ and $\gamma = 1.0$, $\beta = 0.4$ and $M = 2.0$, (d) Graph of variation of horizontal velocity $u$ along $y$-axis at $x = 1$ for various values of $a/c$ and $\gamma = 5.0$, $\beta = 0.4$ and $M = 2.0$.

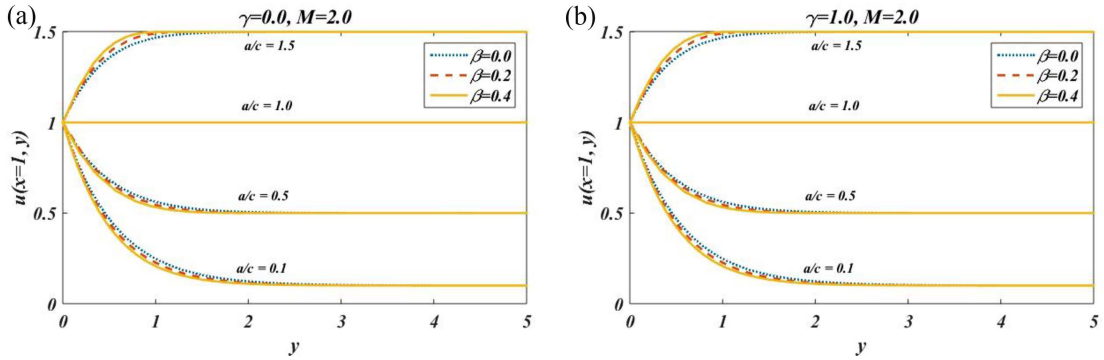


**Fig. 3.** (Color online) (a) Graph of variation of horizontal velocity $u$ along $y$-axis at $x = 1$ for various values of $\beta$ when $a/c = 0.1$, 0.5, 1.0 and 1.5 with $M = 2.0$ for $\gamma = 0.0$ (Orthogonal flow), (b) Graph of variation of horizontal velocity $u$ along $y$-axis at $x = 1$ for various values of $\beta$ when $a/c = 0.1$, 0.5, 1.0 and 1.5 with $M = 2.0$ for $\gamma = 1.0$ (Non-orthogonal flow).

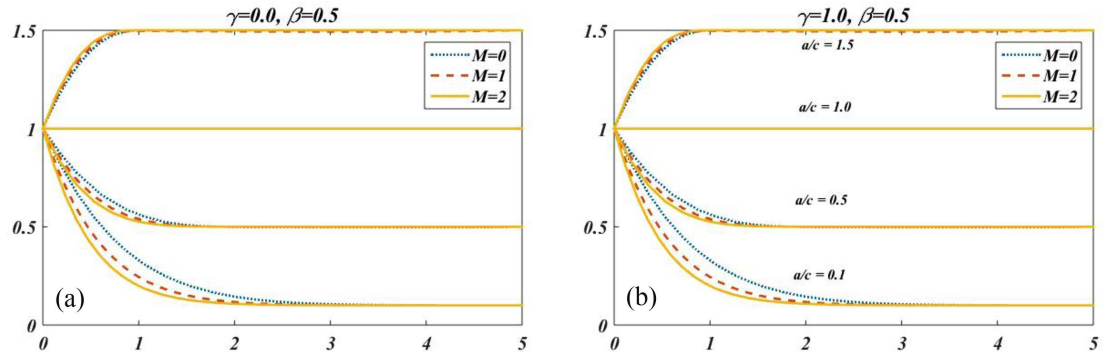


**Fig. 4.** (Color online) (a) Graph of variation of horizontal velocity $u$ along $y$-axis at $x = 1$ for various values of $M$ when $a/c = 0.1$, 0.5, 1.0 and 1.5 with $\beta = 0.5$ for $\gamma = 0.0$ (Orthogonal flow), (b) Graph of variation of horizontal velocity $u$ along $y$-axis at $x = 1$ for various values of $M$ when $a/c = 0.1$, 0.5, 1.0 and 1.5 with $\beta = 0.5$ for $\gamma = 1.0$ (Non-orthogonal flow).

stretching velocities. It is seen that when $a/c > 1$, the flow has normal boundary layer structure but when $a/c < 1$ then the structure shows inverted behavior which is same as reported by Javed and Javed and Ghaffari [5]. It is also noted that the thickness of boundary layer decreases as we increase the value of $a/c$. It is also seen that there exists no boundary layer when $a/c = 1$, its means that viscous effects near the boundary vanishes when both shearing and straining velocities are equal. This behavior is same for both orthogonal and non-orthogonal stagnation point flows. The Figs. 2(a) to 2(d) shows that velocity increases as there is increase in value of $\gamma$. Figure 3(a) and 3(b) is plotted to examine the variational effects of Deborah number $\beta$, for orthogonal flow ($\gamma = 0$) and non-orthogonal flow ($\gamma = 1.0$) with fixed value of $M$ on horizontal velocity $u$. It is seen that by increasing the value of $\beta$ figures show that for inverted boundary layer, the horizontal velocity decreases and thickness of boundary layer decreases but for normal boundary layer the velocity increases and thickness increases for both $\gamma = 0$ and $\gamma = 1$. Figures 4(a) and 4(b) shows the variation effects of magnetic field on the orthogonal stagnation point flow

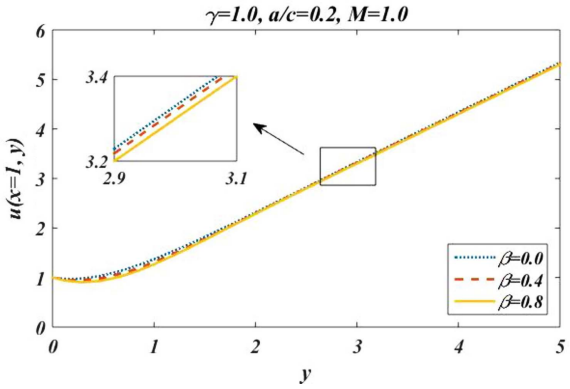


**Fig. 5.** (Color online) Graph of variation of horizontal velocity $u$ along $y$-axis at $x = 1$ for various values of $\beta$ with fixed $a/c = 0.2$ and $M = 1.0$ for $\gamma = 1.0$ (Non-orthogonal flow).

and non-orthogonal point flow respectively for fixed values of $\beta$. It is clear from the figures that by enhancing the magnetic field the horizontal velocity decreases but boundary layer become thinner for inverted boundary but for normal boundary layer the horizontal velocity $u$ increases and boundary layer thickness decreases. Figure 5

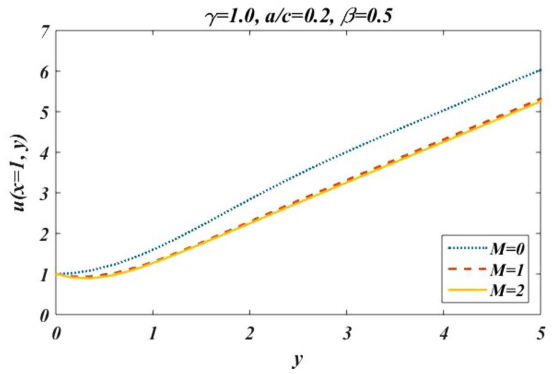


**Fig. 6.** (Color online) Graph of variation of horizontal velocity $u$ along $y$- axis at $x = 1$ for various values of $M$ with fixed $a/c = 0.2$ and $\beta = 0.5$ for $\gamma = 1.0$ (Non-orthogonal flow).

shows that the horizontal velocity decreased when the value of $\beta$ is enhanced by keeping the other parameters fixed. Figure 6 is designed to examine the effects of varying $M$ on horizontal velocity for fixed values of $\gamma$, $a/c$ and $\beta$. Same behavior is observed as that was in the case of effects of $\beta$. But a minor decrease is observed for $M = 1$ and 2. Figures 7(a) and 7(b) shows the streamlines for oblique flow for $a/c = 0.5$ (dashed lines) and 5.0 (solid lines) with fixed $\beta = 4$, $M = 2.0$ and $\gamma = 0.2$ and 2.0, It is seen that by increasing stretching velocity the streamlines more tilted towards left due to increase in straining velocity for $\gamma = 2.0$ but there is no tilted behavior is seen for $\gamma = 0.2$. Figure 8(a) and 8(b) shows treamlines for oblique flow, for $\gamma = -10$ and $-30$ (dashed lines) and 10 and 30 (solid lines) with fixed $\beta = 4$, $M = 2.0$ and $a/$

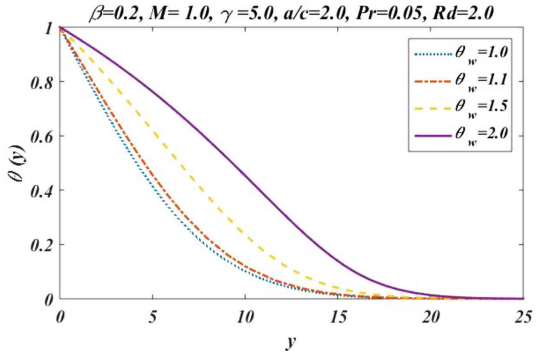


**Fig. 9.** (Color online) Graph of variation of $\theta$ for various values of $\theta_w$ with fixed $\beta = 0.2$, $M = 1.0$, $\gamma = 5.0$, $a/c = 2.0$, $Pr = 0.05$ and $Rd = 2.0$.

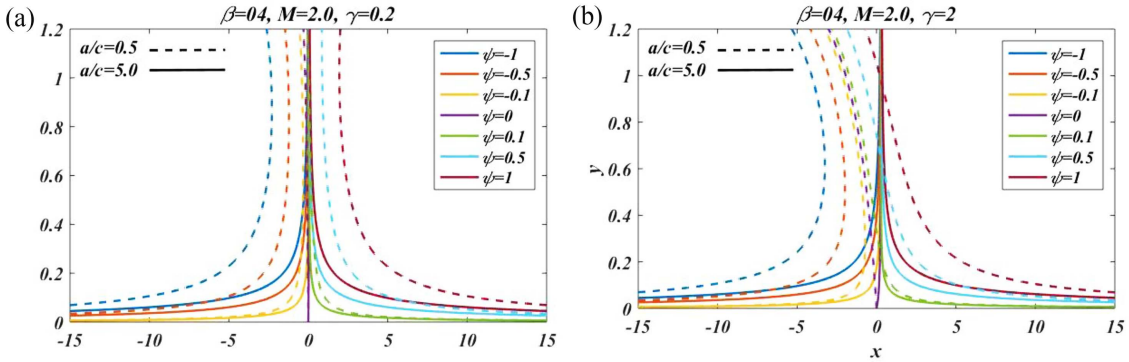


**Fig. 7.** (Color online) (a) Graph of streamlines for oblique flow, for $a/c = 0.5$ (dashed lines) and 5.0 (solid lines) with fixed $\beta = 4$, $M = 2.0$ $\gamma = 0.2$ and $\gamma = 0.2$, (b) Graph of streamlines for oblique flow, for $a/c = 0.5$ (dashed lines) and 5.0 (solid lines) with fixed $\beta = 4$, $M = 2.0$ and $\gamma = 2.0$.

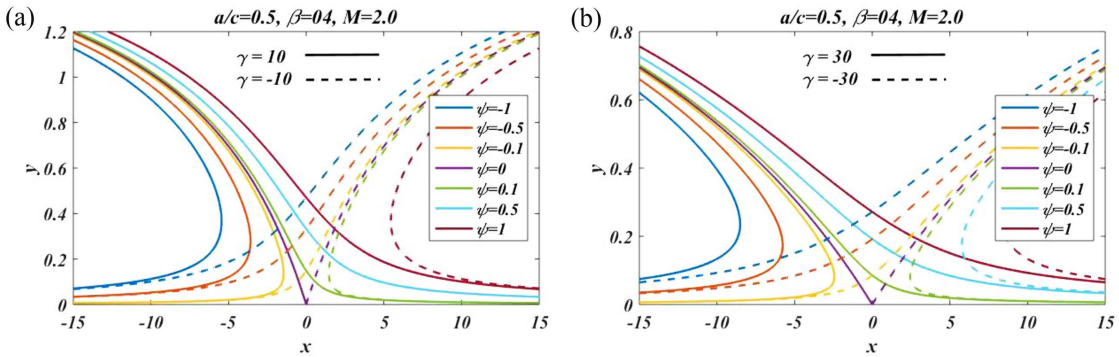


**Fig. 8.** (Color online) (a) Graph of streamlines for oblique flow, for $\gamma = -10$ (dashed lines) and 10 (solid lines) with fixed $\beta = 4$, $M = 2.0$ and $a/c = 0.5$, (b) Graph of streamlines for oblique flow, for $\gamma = -30$ (dashed lines) and 30 (solid lines) with fixed $\beta = 4$, $M = 2.0$ and $a/c = 0.5$.

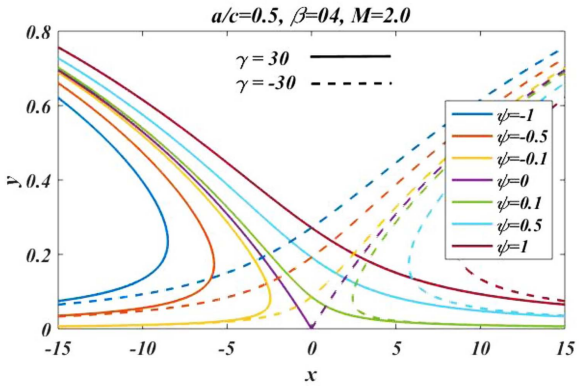


**Fig. 10.** (Color online) Graph of variation of $\theta$ for various values of $Pr$ with fixed $\beta = 0.2$, $M = 1.0$, $\gamma = 5.0$, $a/c = 2.0$, $Rd = 20$ and $\theta_w = 2.0$.

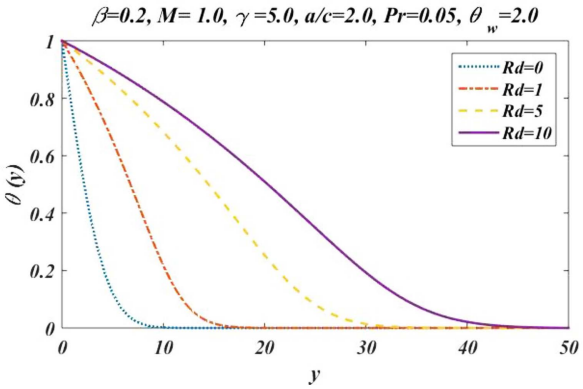


**Fig. 11.** (Color online) Graph of variation of $\theta$ for various values of $Rd$ with fixed $\beta = 0.2$, $M = 1.0$, $\gamma = 5.0$, $a/c = 2.0$, $Pr = 0.05$ and $\theta_w = 2.0$.

$c = 0.5$. It is seen that by increasing the value of $|\gamma|$ results in more obliqueness. Figure 9 is plotted to represent the effects of $\theta_w$ for various values of $\theta_w$ with fixed values of $\beta$, $M$, $\gamma$, $a/c$, $Pr$ and $Rd$. It is seen that the temperature of fluid increases rapidly by increasing the value of surface temperature. A concave curve is seen at $\theta_w = 2.0$. Figure 10 is designed to elaborate the effects of Prandtl number with fixed values of $\beta = 0.2$, $M = 1.0$, $\gamma = 5.0$, $a/c = 2.0$, $Rd = 2.0$ and $\theta_w = 2.0$. It is observed from the figure that the enhancement in the Prandtl number results in decrease in the value of temperature of flow. Figure 11 shows the effects of radiation parameter $Rd$, with fixed values of $\beta = 0.2$, $M = 1.0$, $\gamma = 5.0$, $a/c = 2.0$, $Pr = 0.05$ and $\theta_w = 2.0$. It is observed the by increasing the values of $Rd$ the the temperature of flow increases; also, concave curves are observed for $Rd = 5$ and 10.

## 5. Conclusion

The influence of Hartmann number and radiation parameter on the boundary layer flow of Maxwell fluid in the region of oblique stagnation point over linear stretching sheet is investigated. The participation of the involved parameters are studied by plotting their different variation through graphs and tables. This study concludes increase in the parameter $a/c$ decreases the boundary layer thick of oblique stagnation point flow of non-Newtonian fluid while radiation parameter and surface heating parameter increases the thermal boundary layer thickness By increasing the value of Deborah number for inverted boundary layer, the horizontal velocity decreases and thickness of boundary layer decreases.It is also noted that enhancing the strength of magnetic field, the horizontal velocity decreases but boundary layer becomes thinner. Streamlines shows that increasing the value of $|\gamma|$ results in more obliqueness. Temperature of fluid increases rapidly by increasing the value of surface temperature and radiation parameter $Rd$ but decreases by increasing the Prandtl number.

## Acknowledgements

The authors extend their appreciation to the Deanship of Scientific Research at King Khalid University, Abha 61413, Saudi Arabia for funding this work through research groups program under grant number R.G.P-1-292-1443.

Princess Nourah bint Abdulrahman University Researchers Supporting Project number (PNURSP2022R184), Princess Nourah bint Abdulrahman University, Riyadh, Saudi Arabia.

## References

[1] K. Tamada, J. of the Phy. Society of Japan **46**, 310 (1979).
[2] J. M. Dorrepaal, J. Fluid Mech. **163**, 141 (1986).
[3] I. Husain, F. Labropulu, and I. Pop, Central Europ. J. Phy. **9**, 176 (2011).
[4] S. Wang and W. Tan, Int. J. Heat Fluid Flow **32**, 88 (2011).
[5] T. Javed and A. Ghaffar, Journal of Mechanics **32**, 175 (2016).
[6] S. Mukhopadhyay, Chinese Physics Letters **29**, 054703 (2012).
[7] S. Nadeem, R. U. Haq, and Z. H. Khan, J. of the Taiwan Insti. of Chem. Eng. **45**, 121 (2014).
[8] M. Khan, M. Y. Malik, T. Salahuddin, and F. Khan, J. of the Brazil. Society of Mech. Sci. and Eng. **41**, 138 (2019).
[9] M. Jawad, Z. Shah, S. Islam, J. Majdoubi, I. Tlili, W. Khan, and I. Khan, Symmetry **11**, 207 (2019).
[10] A. Majeed, A. Zeeshan, F. M. Noori, and U. Masud, Mechanics & Industry **20**, 502 (2019).
[11] S. Reza-E-Rabbi, S. F. Ahmed, S. M. Arifuzzaman, T. Sarkar, and M. S. Khan, Eng. Sci. and Tech., An Int. J.

**23**, 605 (2020).
[12] X. Li, A. U. Khan, M. R. Khan, S. Nadeem, and S. U. Khan, Symmetry **11**, 1070 (2019).
[13] F. Ali and A. Zaib, Arab. J. of Basic and Appl. Sci. **26**, 215 (2019).
[14] H. R. Patel, Heliyon **5**, e01555 (2019).
[15] M. G. Sobamowo, A. A. Yinusa, and O. D. Makinde, World Scientific News **138**, 1 (2019).
[16] A. Ghaffari, T. Javed, I. Mustafaand, and F. Labropulu, Thermal Science **23**, 3391 (2019).
[17] N. Vijaya, G. V. R. Reddy, and Y. H. Krishna, Fluid Dyn & Materials Processing **15**, 233 (2019).
[18] T. Javed, H. Ahmad, and A. Ghaffari, Thermal Science **22**, 519 (2018).
[19] W. Ibrahim and M. Negera, J. of the Egyptian Math. Society **28**, 7 (2020).
[20] T. Hayat, S. A. Shehzad, M. Qasim, and S. Obaidat, Zeitschriftfür Naturforschung A **66**, 417 (2011).
[21] A. Mushtaq, S. Abbasbandy, M. Mustafa, T. Hayat, and A. Alsaedi, AIP Advances **6**, 015208 (2016).
[22] F. G. Awad, P. Sibanda, and S. S. Motsa, App. Math. Modelling **34**, 3509 (2010).
[23] S. R. Pop, I. Pop, and T. Grosan, Technische Mechanik-Europ. J. of Eng. Mech. **25**, 100 (2005).
[24] M. Nazeer, F. Hussain, M. I. Khan, A. U. Rehman, E. R. El-Zahar, Y. M. Chu, and M. Y. Malik, Appl. Math. Comput. **420**, 126868 (2022).
[25] Y. M. Chu, B. M. Shankaralingappa, B. J. Gireesha, F. Alzahrani, M. I. Khan, and S. U. Khan, Appl. Math. Comput. **419**, 126883 (2021).
[26] T.-H. Zhao, M. I. Khan, and Y.-M. Chu, Math. Methods Appl. Sci. https://doi.org/10.1002/mma.7310 (2021).
[27] P. Li, A. Abbasi, E. R. El-Zahar, W. Farooq, Z. Hussain, S. U. Khan, M. I. Khan, S. Farooq, M. Y. Malik, and F. Wang, Colloid Interface Sci. Commu. **47**, 100593 (2022).
[28] M. A. Iqbal, Y. Wang, M. M. Miah, and M. S. Osman, Fractal Fract. **6**, 4 (2022).
[29] T.-H. Zhao, Z.-Y. He, and Y.-M. Chu, Comput. Methods Funct. Theory **21**, 413 (2021).
[30] T.-H. Zhao, Z.-Y. He, and Y.-M. Chu, **5**, 6479 (2020).